Korean J. Chem. Eng., **27**(4), 1150-1158 (2010)
DOI: 10.1007/s11814-010-0222-7

Experimental and computational fluid dynamic (CFD) studies on mixing characteristics of a modified helical ribbon impeller

Masoud Rahimi*,†, Aso Kakekhani*, and Ammar Abdulaziz Alsairafi**

*CFD Research Center, Chemical Engineering Department, Razi University, Kermanshah, Iran
**Faculty of Mechanical Engineering, College of Engineering and Petroleum, Kuwait University, Kuwait
(*Received 7 April 2010 • accepted 23 April 2010*)

Abstract−Experimental and computational fluid dynamic (CFD) modeling studies have been performed on mixing characteristics of a new modified helical ribbon impeller in a viscous medium. A novel arrangement for the multiple reference frame (MRF) technique was proposed and the modeling results were compared with those of conventional MRF selecting method. Calculations were performed to study the effects of several parameters: axial flow number, axial circulation time, impeller clearance, and power consumption. The higher performance of the modified impeller has been proven in terms of axial flow number and axial circulation time. The results showed that significant improvement in mixing performance can be obtained at a higher impeller clearance with the modified impeller employed. In addition, the power consumption by the new impeller has been compared with that of the classic one. The CFD-predicted flow patterns generated by the impellers were used to explain the higher performance of the modified impeller. In addition, the results reveal that the CFD-predicted particle volume fractions at various axial distances from the tank bottom are reasonably in agreement with the experimental observations.

Key words: CFD, Helical Ribbon, Hydrodynamics, Mixing, Visualization Mathematical Modeling

INTRODUCTION

The blending of two or more miscible fluids, solid-liquid and gas-liquid mixing are widely encountered in mineral, food, pharmaceutical, polymer, metallurgical, biochemical, and other industrial processes [1,2]. Mixing of viscous fluids is mainly carried out in the laminar and transition regimes. Many impellers were proposed by researchers based either on using large impeller diameter or close-clearance designs like anchors and helical ribbons. The make down of viscous suspensions at high solids content is a unit operation involved in the production of coatings, specialty chemicals, drugs and space fuels. This operation is generally carried out in batch or semi batch mode in stirred vessels. It has been reported that the so-called helical ribbon and helical screw impellers are most appropriate for efficient mixing of high viscosity Newtonian and non-Newtonian liquids [3-5]. However, the power consumption of such impellers is higher compared to those of classic impellers such as Rushton turbines and propellers.

In recent years, the numerical modeling of mixing in a stirred tank (reactor) has attracted a great deal of attention [6]. The quick and vast development of numerical techniques and software abilities can presently take advantage of highly sophisticated engineering techniques such as computational fluid dynamics (CFD) calculation. This has made CFD an important tool for understanding the mixing in the stirred tanks [7]. Nevertheless, modeling of the complex stirred tanks flow in the presence of a rotating impeller is a computational challenge because of the complex geometry of rotating impeller and non-isotropic nature of flow in the stirred tanks. Although CFD commercial codes have made impressive steps towards the solution of such engineering problems over the last decade, it still remains a difficult task to use such codes to help the design and the analysis of stirred tanks.

Iranshahi et al. [8] investigated the flow pattern and mixing progress in a vessel equipped with a Maxblend impeller in the case of viscous Newtonian fluids. In that study, they found that the Maxblend impeller showed good performance when used with baffles in the transition and upper laminar regimes. On another study, a CFD characterization of the hydrodynamics of the Maxblend impeller with viscous Newtonian and non-Newtonian inelastic fluids in the laminar and transition regimes was carried out by Devals et al. [9]. In that study, the effect of the impeller bottom clearance and the Reynolds number on the power characteristic, the distribution of shear rates and the overall flow condition in the vessel were investigated.

Yao et al. [10] performed numerical analysis for the local and total dispersive mixing performance in a stirring tank with a standard type of Maxblend and double helical ribbon impellers. They showed that double Helical Ribbon can not be a promising dispersive mixer.

Iranshahi et al. [11] investigated the fluid flow behavior in a vessel stirring with a Paravisc impeller in the laminar regime using CFD. They compared the viscous mixing characteristics of the Ekato Paravisc with those of an anchor and a double helical ribbon.

A CFD study on the laminar flow and mixing performance in a tank stirred by four Intermig impellers was carried out by Aubin and Xuereb [12]. They investigated the effect of multiple Intermig impeller configuration on mixing performance in a stirred tank.

A numerical modeling was carried out by Bertrand et al. [13] to predict a rise in power draw due to elasticity. They explained the numerical methodology and compared the results of the simulation with experimental data in the case of a tank stirred with a helical ribbon.

†To whom correspondence should be addressed.
E-mail: masoudrahimi@yahoo.com

In another study, CFD modeling was used by Alliet-Gaubert et al. [14] for single-phase flows in multi-stage stirred vessels for two industrial cases. In that study, various methods for results analysis to get a good mixing characterization were collected and the applications of those methods were specified.

Barailer et al. [15] performed a CFD modeling of a rotor-stator mixer in the laminar regime. They investigated the hydrodynamic characteristics of the rotor-stator mixing head in the case of viscous Newtonian fluids.

Another CFD study on behavior of mixing in stirred vessels equipped with anchor type impellers in the laminar regime was carried out by Pedrosa and Nunhez [16], who presented a detailed model of a stirred vessel using Anchor impellers.

Delaplace et al. [17] developed an approximate analytical model based on the Couette flow analogy to predict power consumption for the mixing of pseudoplastic fluids with helical ribbon and helical screw ribbon impellers in the laminar regime. They presented extensive comparisons between the new model predicted results and the data which was reported in the existing literature.

Regarding the above literature survey, the present study has tried to use the MRF technique to model mixing by large impellers, which has been previously modeled using Lagrangian frame of reference. In addition, a modification was done on the well-known helical ribbon impeller to enhance its mixing performance in a high viscosity medium. In the first stage, the classic helical ribbon impeller was modified by installing inclined blades on the impeller-shaft connecting bar. Then, the mixing characteristics of this new impeller were compared with that of the classic helical ribbon impeller. Consequently, the effect of bottom clearance on mixing performance of two impellers was studied. All experiments were modeled using CFD technique and the experimental observations were analyzed.

EXPERIMENTS

In the present study, the experiments were performed in a stirred tank made from Perspex with dimensions shown in Fig. 1. The tank is 14 cm in diameter (T) and a variable liquid height (H) from 14 to 15.6 cm, depending on the impeller bottom clearance. The tank was filled with glycerin solution.

To visualize the mixing performance some polymeric particles

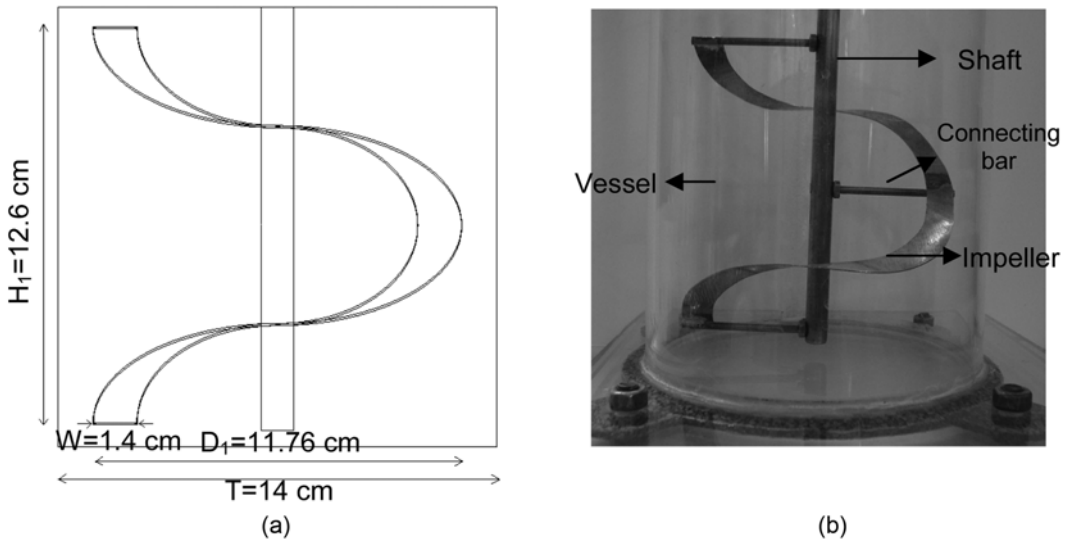

Fig. 1. The mixing vessel. (a) Schematic diagram for the geometrical details, (b) Real view of mixing vessel.

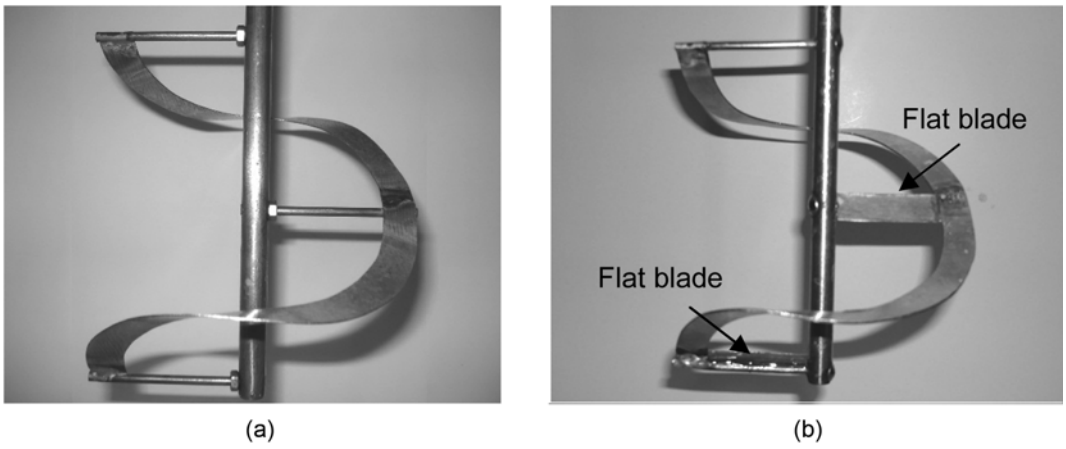

Fig. 2. The classical and modified Helical Ribbon impeller used for study. (a) Classical, (b) Modified.

were used. They are red spherical particles with a diameter of 2.1 mm and a density of 2,500 kg·m^{-3}. In all experiments, the volume fraction of solid was set to be from 1 to 1.2%. A glycerin solution, which was used as the working fluid in the experiments, has a density of 1,258 kg·m^{-3} and a viscosity of 0.6 Pa·s. The roof of vessel was closed by a polymeric plate.

In the present work, a helical ribbon impeller was modified by using two flat blades installed upon the impeller-shaft connecting bars. Fig. 2 illustrates the classic and modified impellers. The connecting bar had a diameter of 3.5 mm and a length of 53.8 mm and new installed blades are 39.8×14×0.7 mm rectangular plates. The angle of blades with horizon was selected to be 45°. This angle was chosen among other angles examined in this research. The impeller is driven by a variable speed motor.

The particle distribution in the mixing tank was studied at four impeller rotational speeds of 100, 130, 145 and 160 rpm. In addition, the particle dispersion at three impeller clearances of 7, 15 and 23 mm (impeller clearance to fluid height ratios of 0.05, 0.1 and 0.15) was studied. In Fig. 3, the front views of particle dispersion using both impellers at various impeller rotational speeds and at the

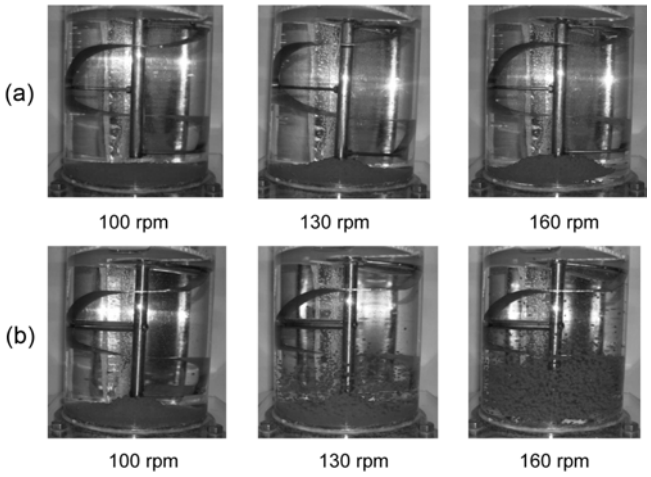

Fig. 3. Experimental visualization of particles spreading in the stirred vessel. (a) Classical, (B) Modified.

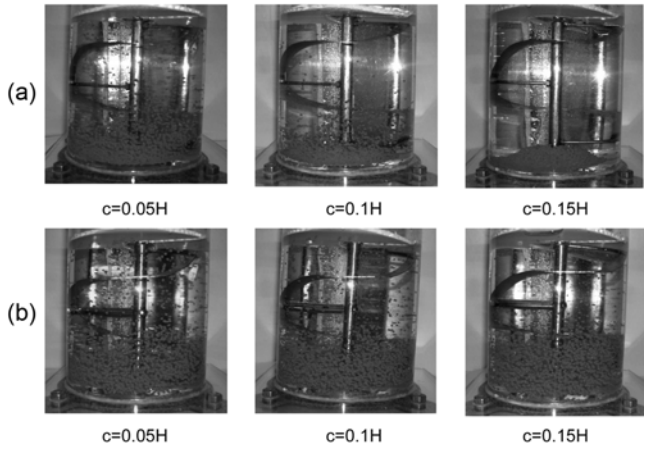

Fig. 4. Experimental visualization of the effect of impeller clearance on mixing quality. (a) Classical, (b) Modified.

impeller clearance of 0.15H are compared. In general, the figure shows that the modified impeller works in a more efficient way in comparison with that of the classic type. These differences are more obvious at higher impeller speed.

1. Effect of Impeller Clearance

Fig. 4 illustrates the particle dispersion at various impeller clearances for both impeller geometries, as the impellers were rotated at 160 rpm. As it can be seen in the pictures, by increasing the impeller clearance the mixing quality has been decreased for both impellers. However, the mixing performance for the modified impeller is higher than the classic one in all clearances studied in this work. It can be seen clearly that there are more differences at higher impeller clearances. This deficiency in the classic type of impeller reach to a situation that particles accumulated at the bottom, close to the middle of the vessel at the clearance of 0.15H. However, at the same clearance the particle dispersion inside the tank is quite significant as the modified impeller was employed.

2. Impeller Power Consumption

In this investigation, the power consumption by both impellers was measured using a torque-meter made by Lutron Company (TQ-8800). To find the impeller power consumption, the following relation was used:

$$P=2\pi NM \tag{1}$$

in which N is the impeller rotational speed and M is the torque applied to the impeller. The power consumption is often represented in dimensionless form by the well known power number, N_p, which has been defined as follow:

$$N_p=\frac{P}{\rho N^3 D^5} \tag{2}$$

In addition, in the field of mixing the Reynolds number has been defined as follows:

$$Re=\frac{\rho ND^2}{\mu} \tag{3}$$

In which N is the impeller rotational speed, D is the impeller diameter, ρ is the liquid density and μ is the fluid viscosity. Therefore, for the employed impeller rotational speeds of 100, 130, 145 and 160 rpm, the corresponding Reynolds numbers are 48, 63, 70 and 77. This confirms that for all cases the fluid flow regime inside the tank is transient close to the laminar.

The measured impellers power consumption in terms of impeller power number and Reynolds number for two clearances are shown in Fig. 5. In general, the figure reveals a decreasing trend in the power number with increasing the impeller speed. In addition, the figure shows that more power is used by the modified impeller in all cases and this is more significant at high impeller clearances. This is quite negligible at the clearance of 0.05H. However, at an impeller clearance of 0.15H, the differences in the power number are more considerable. This may be acceptable considering the significant enhancement in the observed mixing performance illustrated in Fig. 4.

CFD MODELING

The mixing in the studied stirred tank was modeled using commercial CFD code, FLUENT 6.2. The modeling was carried out in

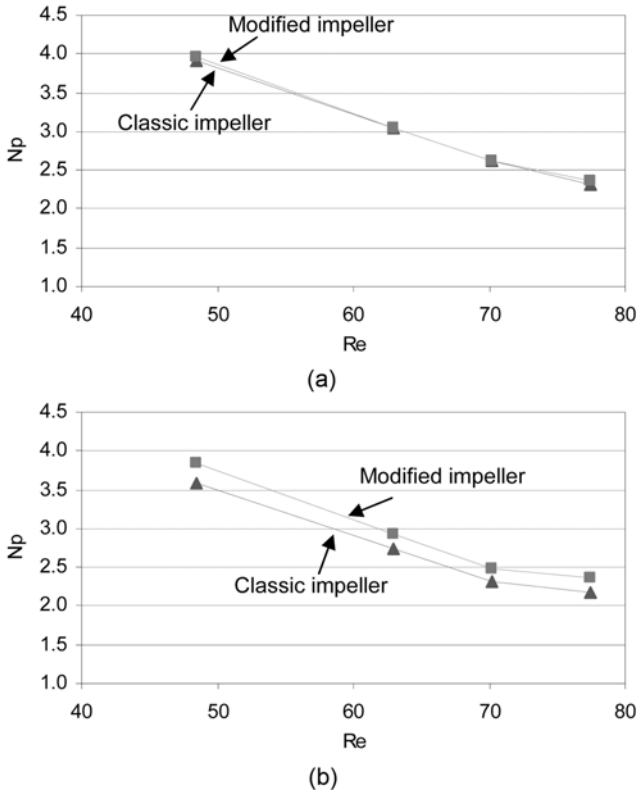

Fig. 5. The impellers power number at two selected impeller clearance. (a) c=0.05H, (b) c=0.15H.

order to predict and explain the experimental observations.

The CFD modeling involves numerical solutions of the conservation equations for mass, momentum and energy. These equations for incompressible flows without energy exchange can be written as follows:

Mass conservation:

$$\frac{\partial \rho}{\partial t} + \nabla \cdot (\rho \vec{u}) = 0 \tag{4}$$

Momentum conservation:

$$\frac{\partial (\rho \vec{u})}{\partial t} + \nabla \cdot (\rho \vec{u}\vec{u}) = \rho g - \nabla P + \nabla \cdot (\tau) \tag{5}$$

Where

$$\tau = \mu \left((\nabla \vec{u} + \nabla \vec{u}^{T}) = \frac{2}{3} \nabla \cdot \vec{u} I \right) \tag{6}$$

Two different approaches are available for the numerical modeling of multiphase flows: the Euler-Lagrange approach and the Euler-Euler approach. In the Euler-Lagrange approach, the fluid phase is treated as a continuum by solving the time-averaged Navier-Stokes equations, while the dispersed phase is solved by tracking a large number of the solid polymeric particles through the calculated flow field based on a force balance on each entity. In the Euler-Euler approach, on the other hand, the different phases have been considered as interpenetrating continuum. Three different Euler-Euler multiphase models are available, including the VOF model, the mixture model and the Eulerian model [18]. The mixture and Eulerian models are appropriate for flows in which the phases are mixed or separated. The Euler-Euler approach and the Eulerian model were employed in the present work.

1. Modeling Strategy

In CFD modeling of a mixing tank the domain involves both stationary (e.g., tank walls) and moving (e.g., impeller) zones. Three modeling methods have been proposed in the literature, including multiple reference frame (MRF), mixing plane method (MPM) and the sliding mesh method (SMM) [18]. The MRF method, proposed by Luo et al. [19], is the simplest one. Two different strategies in selecting the rotating volume were used in the present study and the predicted results were compared with the experiments. In the first MRF layout, a cylinder that surrounds the whole impeller was used as a moving frame. This includes almost 80% of the fluid volume and the rest of the vessel was taken stationary. This is the conventional form of MRF region selection. In the second MRF scheme, two regions in the central part of the vessel were treated as a stationary region. In this scheme, the vessel was divided into three stationary and one moving region. The two schemes are shown in Fig. 6. The main advantage of using the new MRF layout can be expressed in a more efficient way of predicting flow field in the central regions. Therefore, a better prediction of particle spreading in those regions can be achieved. Fig. 7 attempts to show this point by comparing an example of real visualized particle spreading with predicted contour plots of particle distribution using these MRF layouts. Therefore, the whole CFD modeling in this study for different cases is done by using this new MRF layout.

In the present work, the tank was divided into almost 450000 to 500000 unstructured tetrahedral control volumes. The regions close to

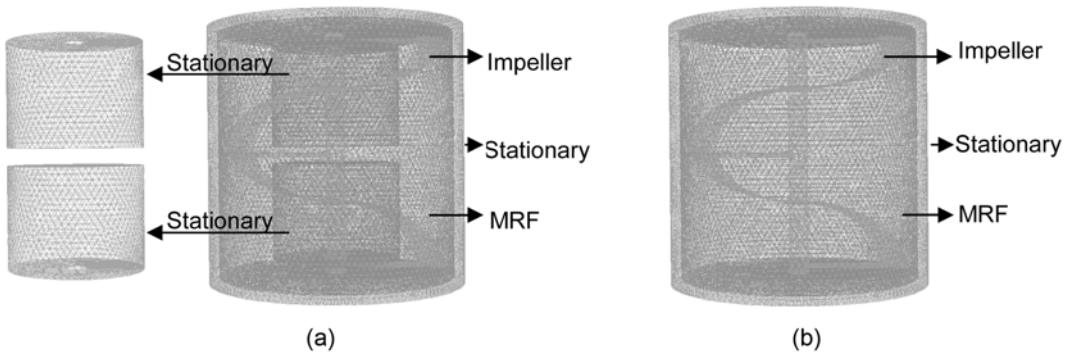

Fig. 6. Two ways of selecting moving frame of reference. (a) Proposed, (b) Conventional.

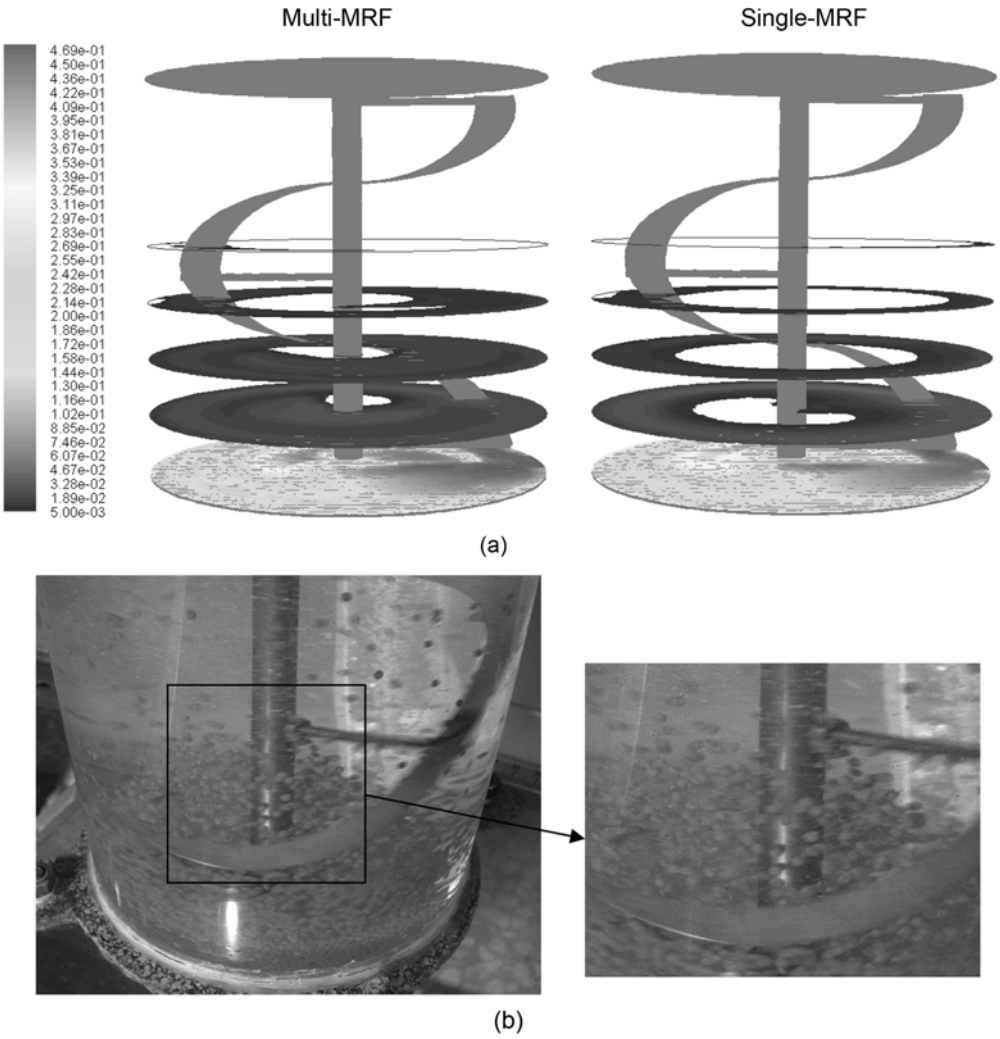

Fig. 7. A comparison between the predicted particles spreading inside the tank using two methods of MRF selecting regions. (a) CFD predicted particle volume fraction inside the tank, (b) Visualization of particle spreading in the tank's central region.

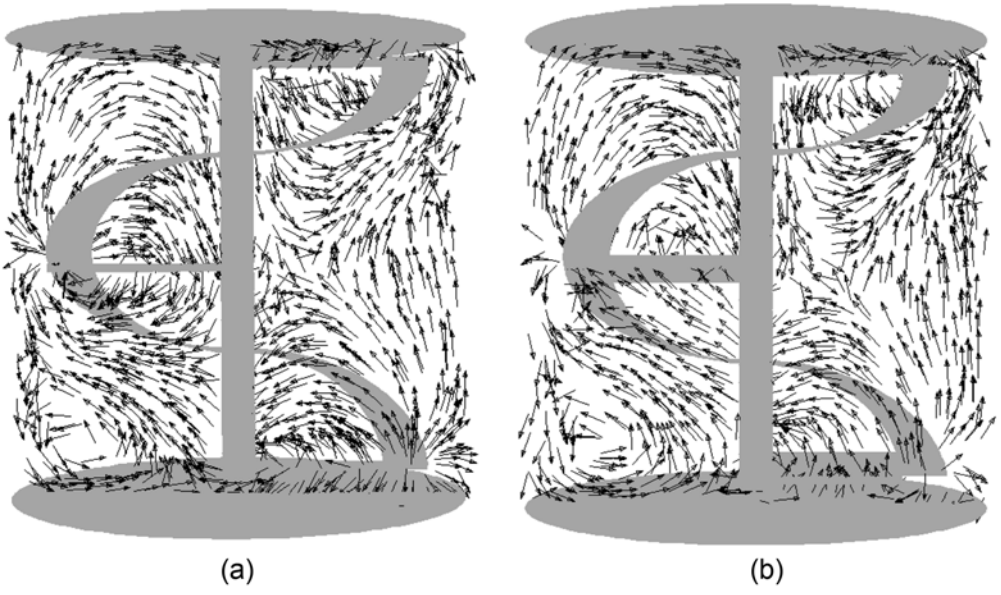

Fig. 8. The generated flow patterns by the two studied impellers. (a) Classic, (b) Modified.

the impeller were meshed into smaller control volumes in order to increase the precision of predictions. The wall condition was considered for the top and bottom of the tank. The phase-coupled SIMPLE pressure-velocity coupling algorithm, the second order upwind discretization scheme for momentum and the first order upwind discretization scheme for volume fractions were employed. The impeller rotation speed was varied between 100 and 160 rpm. Based on this range of the impeller speed, the value of Re number varied from 40 to 80, which can establish a transient flow regime close to laminar. Regarding studies done by Kelly and Gigas [20] and Alliet-Gaubert et al. [14], the macro-instabilities that may happen at this transient flow regime can be neglected, so the flow was assumed laminar. In addition, a convergence criterion of 10^{-7} was chosen for all calculated parameters.

2. CFD Predicted Results

Fig. 8 shows the predicted velocity vectors in an axial slice goes through the middle of the tank for both impeller setups. The figure shows that for both layouts there are two set of loops on the left and right hand sides. In general, these loops push the fluid upward and downward on both sides. However, there are significant differences in the way that fluid circulates inside these loops. On the right hand side and close to the bottom of the tank, a significant part of fluid goes up in the flow generated by modified impeller, while the figure reveals that the flow generated by the classic type both upward and downward flow are at the same level. This is more important on the left hand side, where the modified impeller pushes the fluid upward up to the middle of the tank while in the classic layout the fluid at the same level moves downward.

To find the reason for higher performance of mixing by the modified impeller, the axial flow number and average axial circulating time have been obtained from CFD predicted results. The axial flow rate, Q_{ax}, has been found by the surface integration of the axial velocity component (positive v_z^+ or negative v_z^-) at various horizontal planes inside the vessel as follows:

$$Q_{ax}(z)=\int_A v_z^+ dA=\int_A v_z^- dA \tag{7}$$

In which A is the cell's radial surface area. The average axial flow rate, Q_{Aax}, for the entire vessel has been defined as:

$$Q_{Aax}=\frac{\int_0^H Q_{ax}(z)dz}{\int_0^H dz} \tag{8}$$

Consequently, this average axial flow rate with ND^3 can be used to obtain the dimensionless axial flow number, $N_{Q_{ax}}$, as well as the dimensionless average axial flow number, $N_{Q_{Aax}}$, as follows:

$$N_{Q_{ax}}(z)=\frac{Q_{ax}(z)}{ND^3} \tag{9}$$

$$N_{Q_{Aax}}=\frac{Q_{Aax}}{ND^3} \tag{10}$$

In addition, the following relation defines the average axial circulation time, t_{ax}:

$$t_{ax}=\frac{V}{Q_{Aax}} \tag{11}$$

The axial flow number at various distances from the tank bottom is shown in Fig. 9. In general, the figure shows that the axial fluid flow generated by the modified impeller in lower part of the vessel is higher than that of the classic one. This can be interpreted as the effect of existence of two blades on the impeller. The decreasing trend close to the middle of the tank can be explained by transforming of axial to radial flow, which is due to the axial loops im-

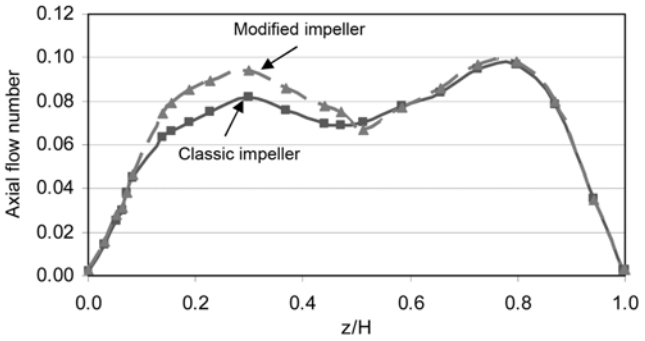

Fig. 9. The axial flow number at different distances from the tank's bottom.

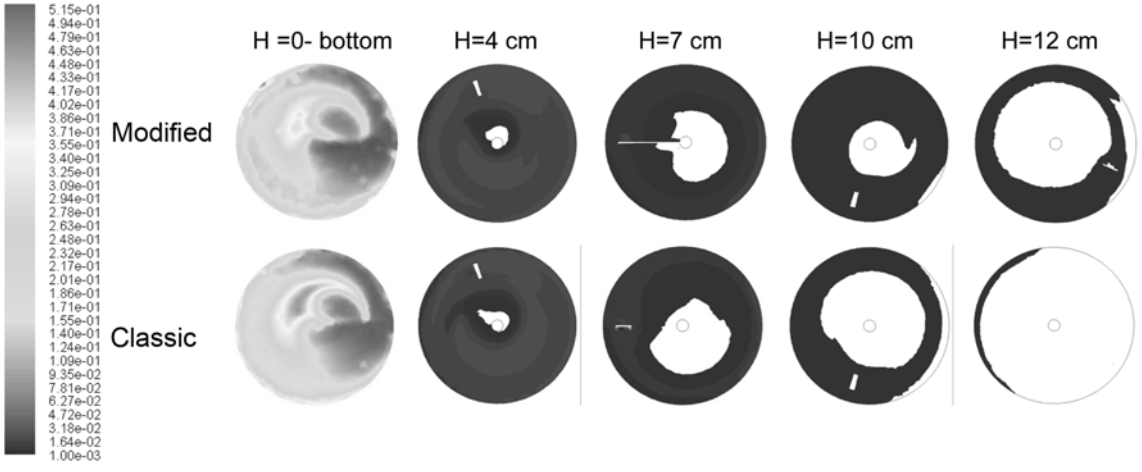

Fig. 10. The particle volume fraction at different axial positions.

pingement in that region.

On other hand, by calculating the $N_{Q_{Aax}}$ and t_{ax} for both geometry, it is obvious to see the role of the new geometry in increasing the mixing performance. The values of 0.0731 and 0.0684 were found for $N_{Q_{Aax}}$ as the modified and classic impeller employed, respectively. According to this calculation the values of 6.80 s and 7.26 s were evaluated for t_{ax}, respectively. These results reveal that the average axial flow number increased by 6.9%, with modified impeller employed. Therefore, the average axial circulation time should decreases by the same order.

Fig. 10 shows the particle fractional volume field in the tank for two setups with the clearance of 0.05H and impeller rotational speed of 160 rpm. The figure illustrates the particle volume fractions in five slices at various axial positions. It is possible to see that more particles can exist at the tank's bottom when the classic impeller is used. However, at higher distance from bottom it is possible to find more particles as the modified impeller is employed. In the last two slices, which are placed in the upper part of the tank, the differences are more obvious.

In the experimental part, it was shown that the modified impeller works in a more efficient way compared with the classic one at higher impeller clearances. To analyze the reason for this observation, the CFD modeling results for maximum and minimum impeller clearances (0.05H and 0.15H) have been analyzed. In the first

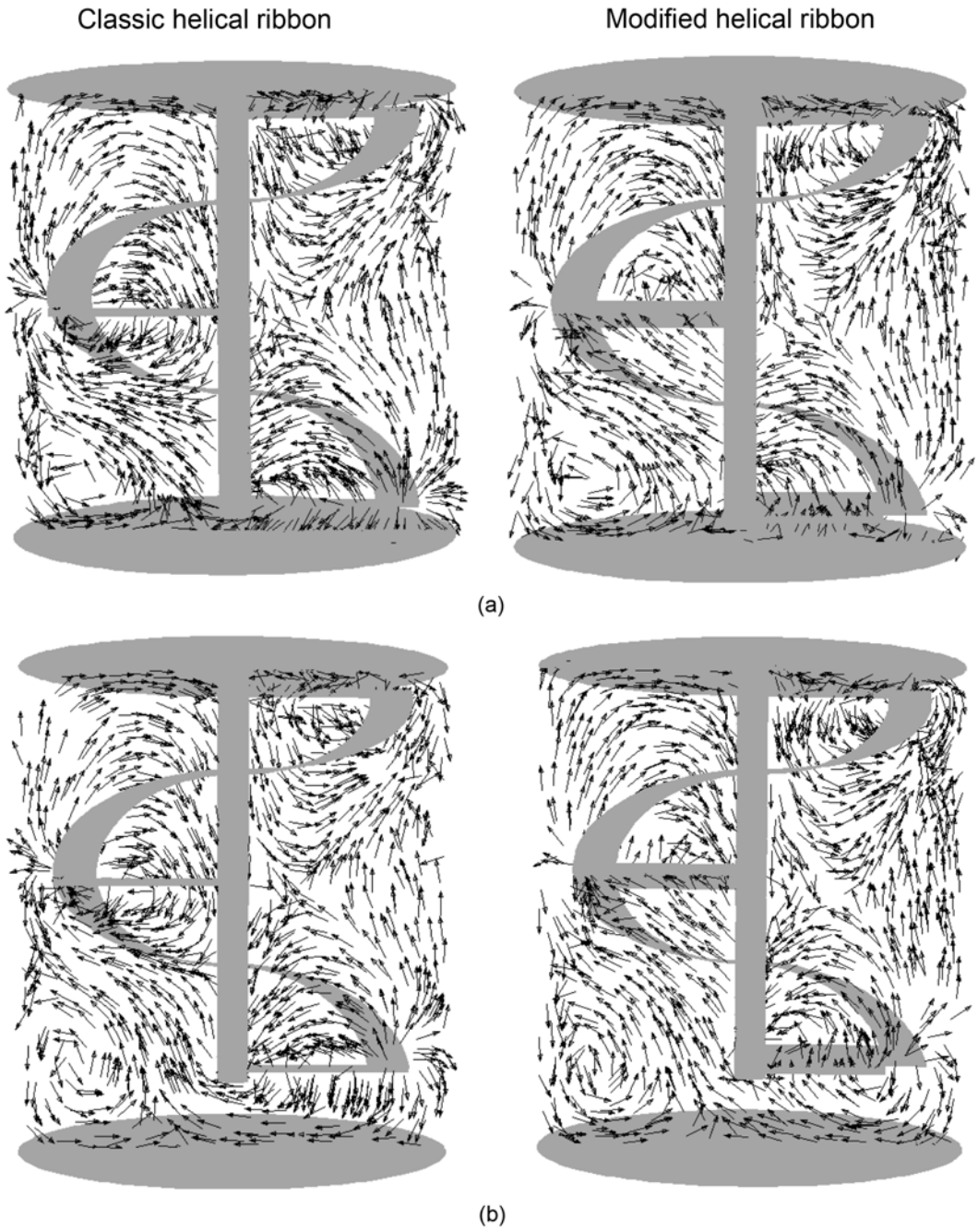

Fig. 11. The flow pattern generated by two impellers at two different impeller bottom clearances. (a) c=0.05H, (b) c=0.15H.

step, flow patterns generated by two setups in a vertical slice going through the middle of the tank are illustrated in Fig. 11. As can be seen, the flow generated by both impellers in the clearance of 0.15H contains more fluid movement close to the tank's bottom. However, in the modified layout there is a circulating loop which pushes the fluid toward the bottom, and then returns it back from the bottom in upward direction. On the other hand, there is not such a flow pattern in the low clearance of 0.05H. This can be interpreted as the main reason for the observed particle dispersion given in Fig. 4.

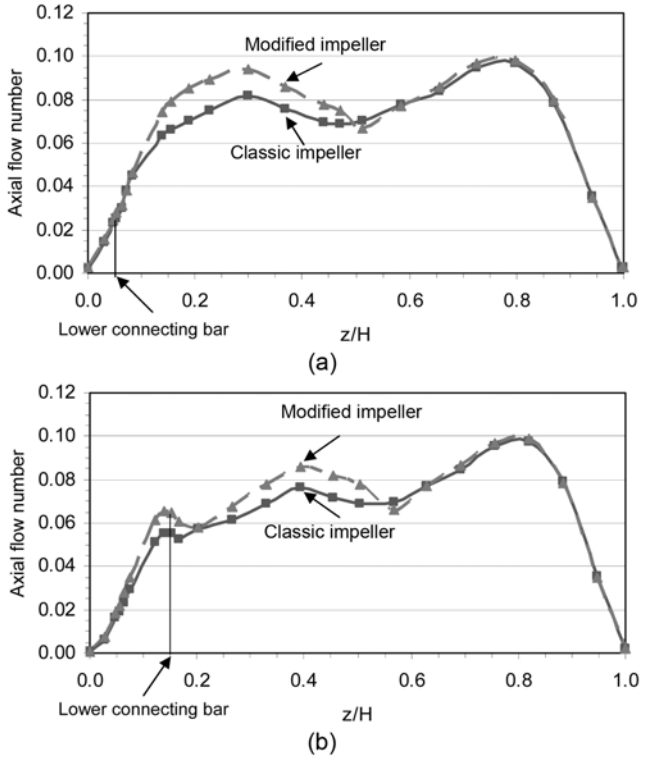

Fig. 12. The predicted axial flow numbers for the impellers at two different impeller clearances. (a) c=0.05H, (b) c=0.15H.

Fig. 12 shows the axial flow number values for the two different impellers at two impeller clearances. The axial flow number has been presented at normalized distances from the tank's bottom. Generally, the figure shows that a higher axial flow number can be obtained by the modified impeller. This causes more particles to have this opportunity to rise from the bottom and join to the flow established above the connecting bar. More quantitatively, turning to Fig. 12(b), which corresponds to a clearance of 0.15H, it is possible to see more differences in the axial flow numbers below the lower connecting bar in comparison with those of clearance of 0.05H. The average value in that region is about 18.4% at clearance of 0.15H. However, the similar calculated value is 7.9% for the clearance of 0.05H. Hence, one may conclude that the modified impeller acts in a more efficient way at a higher clearance.

In the next step, the predicted partial volume fraction in three dimensions has been analyzed. Fig. 13 shows the predicted particle volume fraction in six axial slices up to the middle of the tank for two impeller clearances. In general, the results show that there are more particles at the bottom of tank as the classic impeller is employed. However, by using the modified impeller, more particles have this opportunity to rise toward the upper regions. These differences are more obvious at the predicted results for 0.15H impeller clearance setup, which is quite in agreement with the experimental

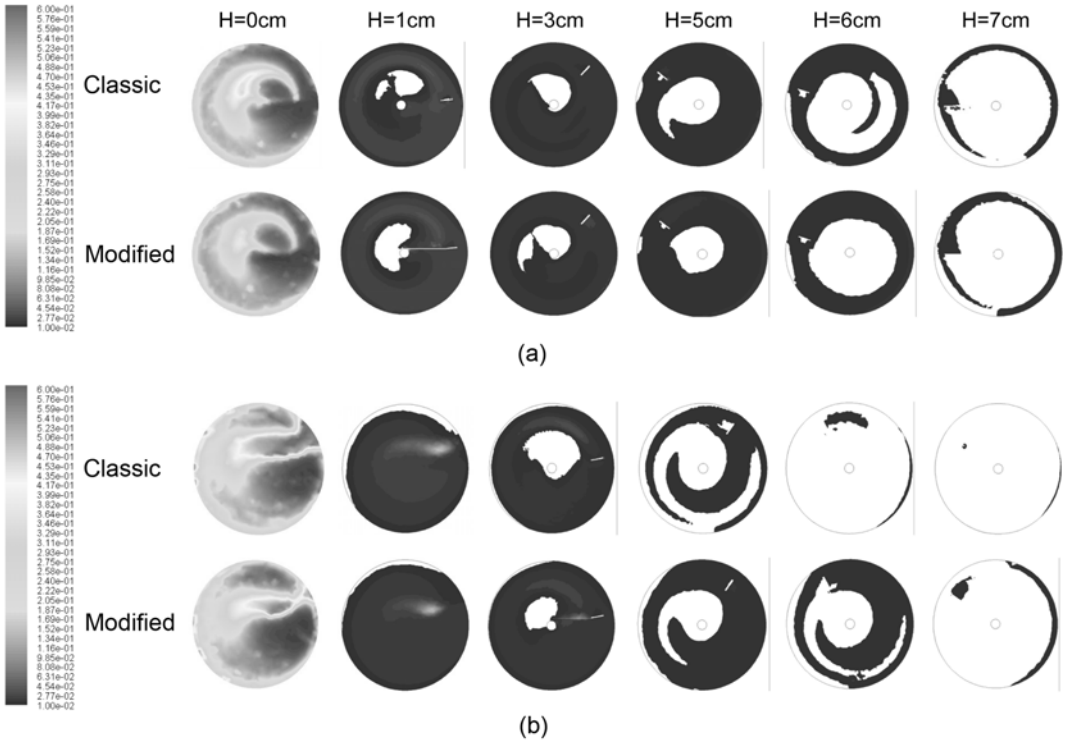

Fig. 13. The particle volume fraction at various axial positions at two impeller clearances. (a) c=0.05H, (b) c=0.15H.

observations given in Fig. 4.

CONCLUSION

This paper deals with a new proposed impeller based on the helical ribbon impeller, which is usually more suitable for mixing in high viscosity medium. Two 45° flat blades were placed upon the shaft-blade connecting bars in order to enhance the upward fluid movement in the tank. Visualization tests were performed on mixing of particles with a density of 2,500 $kg \cdot m^{-3}$ in a glycerin solution. The experiments revealed a higher quality of mixing as the modified impeller was employed. The differences in mixing were more significant at higher impeller clearances. In addition, the power consumption by both impellers was measured and expressed in terms of the power number. Despite significant enhancement in mixing performance, a negligible increase in the power consumption by the modified impeller was observed. In the CFD modeling part, a novel method of using MRF for modeling mixing in stirred tanks was proposed and used. This method may be more reliable for modeling of mixing by large impellers with a high impeller-to-tank diameter ratio. The predicted results using this new MRF layout were in better agreement with that of experimental observation. The predicted flow patterns generated by the two studied impellers were compared in order to explain the experimental observations. In addition, the well-known mixing parameters including axial flow number, average axial flow number and average axial circulation time were calculated. Using these parameters, it has been proved that the modified impeller works in a more efficient way compared with the classic one.

NOMENCLATURE

A : radial cross section of the cell [m^2]
c : bottom clearance [m]
D : impeller diameter [m]
g : gravitational acceleration [$m \cdot s^{-2}$]
H : liquid height in the tank [m]
H_1 : impeller height [m]
I : unit tensor
M : torque [N·m]
N : impeller rotation speed [s^{-1}]
$N_{Q_{Aax}}$: average axial flow number ($=Q_{Aax}/ND^3$)
$N_{Q_{ax}}(z)$: axial flow number ($=Q_{Aax}(z)/ND$)
N_p : power number ($=P/\rho N^3D^5$)
P : agitation power consumption [W]
Q_{Aax} : average axial flow rate [$m^3 \cdot s^{-1}$]
$Q_{ax}(z)$: axial flow rate [$m^3 \cdot s^{-1}$]
r : radial coordinate [m]
Re : Reynolds number ($=\rho ND^2/\mu$)
t_{ax} : average axial circulation time [s]
T : tank diameter [m]
$\vec{u}$: velocity vector [$m \cdot s^{-1}$]
v_z : z-velocity component [$m \cdot s^{-1}$]
V : liquid volume [m^3]
W : impeller width [m]
z : axial coordinate [m]

Greek Letters

μ : fluid viscosity [Pa·s]
ν : kinematic viscosity [$m^2 \cdot s^{-1}$]
ρ : density [$kg \cdot m^{-3}$]
τ : stress tensor [Pa]
ω : angular velocity [$rad \cdot s^{-1}$]

REFERENCES

1. S. H. Kim, A. Bidkar, H. H. Ngo, S. Vigneswaran and H. Moon, *Korean J. Chem. Eng.*, **18**, 163 (2001).
2. S. G. Kim, K. J. Choi, P. J. Yu, S. H. Kim, Y. D. Lee, *Korean J. Chem. Eng.*, **25**, 19 (2008).
3. L. Fradette, P. A. Tanguy, F. Bertrand, F. Thibault, J. B. Ritz and E. Giraud, *Comput. Chem. Eng.*, **31**, 334 (2007).
4. R. P. Chhabra, *Adv. Heat Trans.*, **37**, 77 (2003).
5. R. P. Chhabra and J. F. Richardson, *Non-newtonian flow in the process industries*, Butterworth-Heinemannm, Oxford (1999).
6. J. E. Pérez-Terrazas, V. Ibarra-Junquera and H. C. Rosu, *Korean J. Chem. Eng.*, **25**, 461 (2008).
7. B. H. Um and T. R. Hanley, *Korean J. Chem. Eng.*, **25**, 1094 (2008).
8. A. Iranshahi, C. Devals, M. Heniche, L. Fradette, P. A. Tanguy and K. Takenaka, *Chem. Eng. Sci.*, **62**, 3641 (2007).
9. C. Devals, M. Heniche, K. Takenaka and P. A. Tanguy, *Comput. Chem. Eng.*, **32**, 1831 (2008).
10. W. Yao, M. Mishima and K. Takahashi, *Chem. Eng. J.*, **84**, 565 (2001).
11. A. Iranshahi, M. Heniche, F. Bertrand and P. A. Tanguy, *Chem. Eng. Sci.*, **61**, 2609 (2006).
12. J. Aubin and C. Xuereb, *Chem. Eng. Sci.*, **61**, 2913 (2006).
13. F. Bertrand, P. A. Tanguy, E. B. Fuente and P. Carreau, *Comput. Methods in Appl. Mech. Eng.*, **180**, 267 (1999).
14. M. Alliet-Gaubert, R. Sardeing, C. Xuereb, P. Hobbes, B. Letellier and P. Swaels, *Chem. Eng. Process.*, **45**, 415 (2006).
15. F. Barailler, M. Heniche and P. A. Tanguy, *Chem. Eng. Sci.*, **61**, 2888 (2006).
16. S. M. C. P. Pedrosa and J. R. Nunhez, *Comput. Chem. Eng.*, **24**, 1745 (2000).
17. G. Delaplace, R. Guerin, J. Leuliet and R. P. Chhabra, *Chem. Eng. Sci.*, **61**, 3250 (2006).
18. FLUENT 6.2 ®; FLUENT Inc.: Lebanon, NH, USA (2005).
19. J. Y. Luo, R. I. Issa and A. D. Gosman, *Prediction of impeller-induced flows in mixing vessels using multiple frames of reference*, Proceeding of Institution of Chemical Engineers, Symposium Series no. 136, U.K, 549-556 (1993).
20. W. Kelly and B. Gigas, *Chem. Eng. Sci.*, **58**, 2141 (2003).